



A Fast Matrix Solver for Linear Boundary-Value Problem in the PEM Fuel Cell Impedance Model

Andrei Kulikovsky 1,2,z

A core physics-based model for PEM fuel cell impedance reduces to the numerical solution of a boundary value problem for two coupled, linear, complex-valued ordinary differential Eqs. with variable coefficients. We report a matrix formulation of a previously developed recurrent method for the fast numerical solution of this problem. This formulation does not require iterations and it utilizes only elementary functions and 4×4 matrix products, resulting in one to two orders of magnitude faster code compared to the standard Python boundary-value problem solver. This significantly improves the computational speed of the physics-based impedance model, making it competitive with the popular equivalent circuit modeling approach. The numerical calculation of cell impedance is demonstrated based on the model that includes proton transport in the catalyst layer and oxygen transport in the catalyst and gas-diffusion layers. Least–squares fitting of a real experimental spectrum shows that the matrix solver returns the cell transport parameters 50 times faster than the classic boundary-value problem solver.

© 2024 The Author(s). Published on behalf of The Electrochemical Society by IOP Publishing Limited.. This is an open access article distributed under the terms of the Creative Commons Attribution 4.0 License (CC BY, http://creativecommons.org/licenses/by/4.0/), which permits unrestricted reuse of the work in any medium, provided the original work is properly cited. [DOI: 10.1149/2754-2734/ad6ce8]

Manuscript submitted May 13, 2024; revised manuscript received July 22, 2024. Published August 19, 2024.

List of Symbols

	Dist of Symbols
~	Marks dimensionless variables
a_n, b_n	Sub-layer boundaries, Fig. 1
b_T	ORR Tafel slope, V
C_{dl}	Double layer volumetric capacitance, F cm ⁻³
c	Oxygen molar concentration in the CCL, mol cm^{-3}
c_g	Oxygen molar concentration in the GDL, mol cm^{-3}
c_{ref}	Reference oxygen concentration, mol cm ⁻³
D_{ox}	Oxygen diffusion coefficient in the CCL, cm ² s ⁻¹
D_g	Oxygen diffusion coefficient in the GDL film, cm ² s ⁻¹
F	Faraday constant, C mol ⁻¹
i*	ORR volumetric exchange current density, A cm ⁻³
i	Imaginary unit
j	Local proton current density in the CCL, A cm ⁻²
j_0	Cell current density, A cm ⁻²
l_t	CCL thickness, cm
$\stackrel{\cdot}{N} \\ \tilde{N}^1$	Number of sub-layers
	$=\partial \tilde{c}^1/\partial \tilde{x}$
$P_{\eta}, Q_{\eta}, R_{\eta}, S_{\eta},$	
P_c , Q_c , R_c , S_c ,	
P_q, Q_q, R_q, S_q	C CC : 4 : E 11.34
P_j, Q_j, R_j, S_j	Coefficients in Eq. 11, 34
p, q, r, s	Dimensionless coefficients, Eq. 7
q^*	Dimensionless parameter, Eq. 24
X Subsavinta	Coordinate through the cathode, cm
Subscripts: a, b	$\tilde{x} = a \text{ or } \tilde{x} = b, \text{ respectively}$
	x = u of $x = b$, respectively GDL
$g \\ 0$	Membrane/CCL interface
1	CCL/GDL interface
Superscripts:	CCE/GDE interface
0	Steady-state value
1	Small–amplitude perturbation
Greek:	party perturbation
α	Dimensionless parameter, Eq. 25

Dimensionless Newman's reaction penetration

ORR overpotential, positive by convention, V

μ	Dimensionless parameter, Eq. 8
σ_p	Nafion film proton conductivity, S cm ⁻¹
$\hat{\omega}$	Angular frequency of the AC signal, s ⁻¹

Electrochemical impedance spectroscopy proved to be an indispensable tool for in situ and in operando PEM fuel cells diagnostics. Every transport and kinetic process running in the cell typically has its own "resonance" frequency; variation of applied AC signal frequency over several decades allows one to probe virtually all the processes.

Extraction of transport and kinetic coefficients requires fitting of a relevant model to experimental impedance spectra. Due to its simplicity, a method of equivalent circuit has been widely used in fuel cell literature. However, any selected equivalent circuit is not unique, which could lead to misleading results. More recent techniques for spectra analysis are the distribution of relaxation times (DRT) and the distribution of diffusion times (DDT). The DRT is based on expansion of impedance spectrum over an infinite sum of parallel *RC*-circuit impedances, while the DDT employs impedance expansion over elementary diffusion impedances. Unfortunately, due to *interdependence* discussed below, none of the aforementioned methods allow for reliable extraction of physical cell parameters from the impedance spectra.

In PEM fuel cell, one of the key problems is understanding potential loss due to oxygen transport from the cathode channel inlet to catalyst sites in the cathode catalyst layer (CCL). Calculations using the physics-based analytical model shows that the individual contributions of channel, gas—diffusion layer and CCL into the total oxygen transport impedance cannot be separated by means of DRT. The problem is that the individual impedances of oxygen transport in the chain of channel, GDL and CCL depend on each other, i.e., changing the transport parameter of any chain element affects impedances of the other elements. The only exclusion is proton transport in the CCL, which is well separated from the other processes by one to two frequency decades gap. Since the DDT differs from the DRT by the form of expansion kernel only, the same interdependence problem is expected to exist in the DDT technique.

From the author's perspective, the most reliable technique for deciphering impedance is fitting of one of the developed over the past three decades physics–based impedance (PBI) models 11-30

depth, Eq. 8

¹ Forschungszentrum Jülich GmbH, Theory and Computation of Energy Materials (IET–3), Institute of Energy and Climate Research, D–52425 Jülich, Germany

²Lomonosov Moscow State University, Research Computing Center, 119991 Moscow, Russia

(see also review³¹) to the spectra. In PEMFC impedance problems, an answer to the question raised by Boukamp in the title of his paper⁸ seems to be negative: neither DRT, nor DDT can replace least–squares fitting of PBI models to experiment. On the other hand, DDT proved to be useful for analysis of spectra from single catalyst layers.⁹

The use of PBI technique is limited by complexity and slowness of PBI models, which involve numerical solution of a boundary–value problem. The simplest (and in many cases quite relevant) PBI model is based on the proton charge and oxygen mass conservation Eqs. in the CCL (Basic transport equations Section). The model enables simple incorporation of oxygen transport in the gas diffusion layer (GDL) impedance (Matrix formulation Section). Fitting of this core impedance model to experimental spectra includes multiple (for each frequency point) numerical solutions of a boundary-value problem (BVP) for a system of linear complex-valued ordinary differential Eqs. (ODEs) for the small perturbation amplitudes.

Recently, a fast recurrent method for solution of this problem has been suggested. ³³ Below, the method ³³ is reformulated in a compact matrix form, which significantly improves the speed of spectra calculations. The matrix formulation allows to perform least–squares fitting of the PBI model to experimental spectrum in less than a second on a standard notebook. This makes the core PBI model a fast and reliable alternative to the equivalent circuit models.

Model

Basic transport equations.—For the sake of completeness, in this and next Sections we give a brief schematic of derivation of recurrent relations³⁴ forming the basis for the matrix method. The PEMFC impedance model discussed here employs a classic system of macro–homogeneous Eqs. for the CCL performance. The system includes the time–dependent proton charge– and oxygen mass–conservation equations:³³

$$C_{dl}\frac{\partial \eta}{\partial t} - \sigma_p \frac{\partial^2 \eta}{\partial x^2} = -i_* \left(\frac{c}{c_{ref}}\right) \exp\left(\frac{\eta}{b_T}\right),$$
[1]

$$\frac{\partial c}{\partial t} - D_{ox} \frac{\partial^2 c}{\partial x^2} = -\frac{i_*}{4F} \left(\frac{c}{c_{ref}}\right) \exp\left(\frac{\eta}{b_T}\right).$$
 [2]

Here t is time, x is the coordinate through the cell counted from the membrane (Fig. 1), η is the positive by convention oxygen reduction reaction (ORR) overpotential, C_{dl} is the volumetric double layer capacitance (F cm⁻³), σ_p is the CCL proton conductivity, b_T is the ORR Tafel slope, i_* is the ORR exchange current density, c is the local oxygen concentration in the CCL, c_{ref} is the reference oxygen concentration, D_{ox} is the effective oxygen diffusion coefficient in the CCL, and F is the Faraday constant. The right side of Eqs. 1, 2 is the Tafel ORR rate.

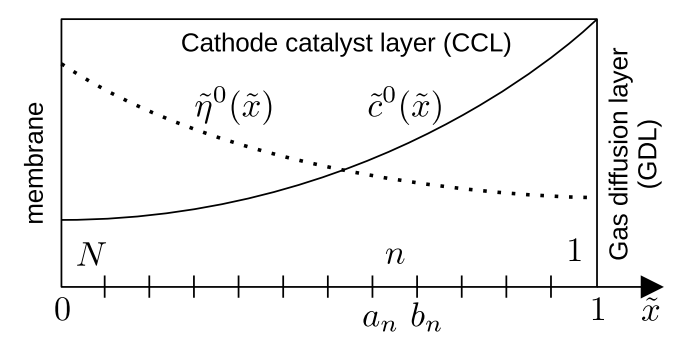


Figure 1. Schematic of the cathode catalyst layer separated into N sub–layers and the characteristic shapes of the static oxygen concentration \tilde{c}^0 and ORR overpotential $\tilde{\eta}^0$. The problem (9), (10) is solved on a single sub–layer $[a_n, b_n]$. Note that the sub–layers are numbered from the GDL/CCL interface toward the membrane.

Linearization and Fourier transform of Eqs. 1, 2 includes the following steps (for further derivation details see³³):

- Substitute $\tilde{\eta}(\tilde{x},\tilde{t}) = \tilde{\eta}^0(\tilde{x}) + \tilde{\eta}^1(\tilde{x},\tilde{t})$ and $\tilde{c}(\tilde{x},\tilde{t}) = \tilde{c}^0(\tilde{x}) + \tilde{c}^1(\tilde{x},\tilde{t})$ into Eqs. 1, 2 and perform linearization assuming $\tilde{\eta}^1 \ll \tilde{\eta}^0$, $\tilde{c}^1 \ll \tilde{c}^0$. Here the superscripts 0 and 1 mark the static variables and the small perturbation amplitudes, respectively, Expand the right side of Eqs. 1, 2 in Taylor series over $\tilde{\eta}^1$ and \tilde{c}^1 keeping two leading terms and neglecting the terms with perturbation products. Subtract the static Eqs. for $\tilde{\eta}^0$ and \tilde{c}^0 , which are obtained from Eqs. 1, 2 by chalking out the terms with time derivatives.
- Substitute Fourier–transformations $\tilde{\eta}^1(\tilde{x}, \tilde{t}) = \tilde{\eta}^1(\tilde{x}, \tilde{\omega}) \exp(i\tilde{\omega}\tilde{t})$ and $\tilde{c}^1(\tilde{x}, \tilde{t}) = \tilde{c}^1(\tilde{x}, \tilde{\omega}) \exp(i\tilde{\omega}\tilde{t})$ into the linearized equations. This leads to linear BVPs for the perturbation amplitudes $\tilde{\eta}^1(\tilde{x}, \tilde{\omega})$ and $\tilde{c}^1(\tilde{x}, \tilde{\omega})$:

$$\frac{\partial^2 \tilde{\eta}^1}{\partial \tilde{x}^2} = p\tilde{c}^1 + q\tilde{\eta}^1, \quad \tilde{\eta}^1(1) = \tilde{\eta}_1^1, \quad \frac{\partial \tilde{\eta}^1}{\partial \tilde{x}} \bigg|_{\tilde{z}} = 0$$
 [3]

$$\frac{\partial^2 \tilde{c}^1}{\partial \tilde{x}^2} = r\tilde{c}^1 + s\tilde{\eta}^1, \quad \frac{\partial \tilde{c}^1}{\partial \tilde{x}} \bigg|_{\tilde{c}=0} = 0, \quad \tilde{c}^1(1) = \tilde{c}_1^1$$
 [4]

Here, ω is the angular frequency of applied AC signal, and the dimensionless variables are defined according to

$$\tilde{t} = \frac{t}{t_*}, \quad \tilde{x} = \frac{x}{l_t}, \quad \tilde{c} = \frac{c}{c_{ref}}, \quad \tilde{\eta} = \frac{\eta}{b_T}, \quad \tilde{j} = \frac{j}{j_*},$$

$$\tilde{D} = \frac{4FDc_{ref}}{\sigma_p b_T}, \quad \tilde{\omega} = \omega t_*, \quad \tilde{Z} = \frac{Z\sigma_p}{l_t}.$$
[5]

where the characteristic time and current density are

$$t_* = \frac{C_{dl}b_T}{i_*}, \quad j_* = \frac{\sigma_p b_T}{l_t}.$$
 [6]

The boundary conditions in Eq. 3 fix applied potential perturbation $\tilde{\eta}_1^1$ at the CCL/GDL interface ($\tilde{x}=1$) and zero proton current through this interface. The b.c. for Eq. 4 mean zero oxygen flux in the membrane and fixed oxygen concentration perturbation \tilde{c}_1^1 prescribed by oxygen transport in the GDL at $\tilde{x}=1$ (see below).

The coefficient functions p, q, r, s are given by

$$p = \frac{e^{\tilde{\eta}^0}}{\varepsilon^2}, \quad q = \frac{\tilde{c}^0 e^{\tilde{\eta}^0} + i\tilde{\omega}}{\varepsilon^2},$$

$$r = \frac{e^{\tilde{\eta}^0} + i\tilde{\omega}\mu^2}{\varepsilon^2 \tilde{D}_{or}}, \quad s = \frac{\tilde{c}^0 e^{\tilde{\eta}^0}}{\varepsilon^2 \tilde{D}_{or}}.$$
[7]

where ε and μ are the dimensionless parameters

$$\varepsilon = \sqrt{\frac{\sigma_p b_T}{i_* l_t^2}}, \quad \mu = \sqrt{\frac{4F c_{ref}}{C_{dl} b_T}}.$$
 [8]

At low cell currents, the coefficients p, q, r, s are nearly constant along \tilde{x} , allowing analytical solution to the problem (3), (4). However, at practically relevant currents, $e^{\tilde{\eta}^0}$ and \tilde{c}^0 strongly vary with \tilde{x} , and the problem (3), (4) could only be solved numerically. The standard Python BVP solver $solve_bvp$ easily integrates this problem; however, the process is slow for using in the spectra fitting algorithms. Fitting includes multiple solution of Eqs. 3, 4 for several tens of frequency points ω (typically \gtrsim 50) and the speed of Eqs. 3, 4 numerical integration plays a pivotal role.

Recurrent method.—A faster numerical method for Eqs. 3, 4 solution is based on the following idea.³⁴ We separate the domain $\tilde{x} \in [0, 1]$ into N sub-intervals numbered from the CCL/GDL

interface to the membrane (Fig. 1). Further, we approximate the static shapes $\tilde{\eta}^0(\tilde{x})$ and $\tilde{c}^0(\tilde{x})$ by stepwise functions, i.e. on each sub-interval, $\tilde{\eta}^0$ and \tilde{c}^0 are constant. With this, Eqs. 3, 4 for a single interval $[a_n, b_n]$ (Fig. 1) can be reformulated as a Cauchy problem (until the end of this section, the subscript *n* is omitted):

$$\frac{\partial^2 \tilde{\eta}^1}{\partial \tilde{x}^2} = p\tilde{c}^1 + q\tilde{\eta}^1, \quad \tilde{\eta}^1(b) = \tilde{\eta}_b^1, \quad \frac{\partial \tilde{\eta}^1}{\partial \tilde{x}} \bigg|_{\tilde{z}=b} = -\tilde{j}_b^1, \quad [9]$$

$$\frac{\partial^2 \tilde{c}^1}{\partial \tilde{x}^2} = r\tilde{c}^1 + s\tilde{\eta}^1, \quad \tilde{c}^1(b) = \tilde{c}_b^1, \quad \frac{\partial \tilde{c}^1}{\partial \tilde{x}} \bigg|_{\tilde{c}=b} = \tilde{N}_b^1.$$
 [10]

In Eqs. 9, 10, all the boundary (initial) conditions are set at $\tilde{x} = b$. Analytical solution to the linear problem (9), (10) with constant coefficients is straightforward. Setting $\tilde{x} = a$ in the solution, we get linear algebraic Eqs. relating the unknown functions at $\tilde{x} = a$ with their values at $\tilde{x} = b$ (Fig. 1):

$$\begin{split} \tilde{\eta}_{a}^{1} &= P_{\eta} \tilde{\eta}_{b}^{1} + Q_{\eta} \tilde{c}_{b}^{1} + R_{\eta} \tilde{N}_{b}^{1} + S_{\eta} \tilde{j}_{b}^{1} \\ \tilde{c}_{a}^{1} &= P_{c} \tilde{\eta}_{b}^{1} + Q_{c} \tilde{c}_{b}^{1} + R_{c} \tilde{N}_{b}^{1} + S_{c} \tilde{j}_{b}^{1} \\ \tilde{N}_{a}^{1} &= P_{q} \tilde{\eta}_{b}^{1} + Q_{q} \tilde{c}_{b}^{1} + R_{q} \tilde{N}_{b}^{1} + S_{q} \tilde{j}_{b}^{1} \\ \tilde{j}_{a}^{1} &= P_{i} \tilde{\eta}_{b}^{1} + Q_{i} \tilde{c}_{b}^{1} + R_{i} \tilde{N}_{b}^{1} + S_{i} \tilde{j}_{b}^{1}, \end{split}$$
[11]

where we keep notations.³⁴ The explicit expressions for the coefficients in Eq. 11 though p, q, r, s can be found in Ref. 34. Starting from the values at the CCL/GDL interface (at $\tilde{x} = 1$)

$$\tilde{\eta}_{h}^{1}(1) = \tilde{\eta}_{1}^{1}, \quad \tilde{c}_{h}^{1}(1) = \tilde{c}_{1}^{1}, \quad \tilde{j}_{h}^{1}(1) = 0, \quad \tilde{N}_{h}^{1}(1) = \tilde{N}_{1}^{1}$$
 [12]

and applying Eq. 11 N times, we get the solution at the membrane interface $\tilde{\eta}_a^1(0)$, $\tilde{c}_a^1(0)$, $\tilde{j}_a^1(0)$, $\tilde{N}_a^1(0)$. The system impedance is

$$\tilde{Z} = \frac{\tilde{\eta}_a^1(0)}{\tilde{j}_a^1(0)} \equiv \frac{\tilde{\eta}_N^1}{\tilde{j}_N^1}$$
 [13]

Note that the initial parameter \tilde{N}_1^1 (the derivative $\partial \tilde{c}^1/\partial \tilde{x}$ at $\tilde{x}=1$) in Eq. 12 is yet undefined. This parameter must provide $\tilde{N}_N^1 = 0$ (zero oxygen flux in the membrane). In Ref. 34, relatively slow calculation of \tilde{N}_1^1 using Eq. 11 and the iterative SciPy solver *fsolve* has been suggested.

Matrix formulation.—Equation 11 can be written in the matrix form as

$$\begin{pmatrix} \tilde{\eta}_{a}^{1} \\ \tilde{c}_{a}^{1} \\ \tilde{N}_{a}^{1} \\ \tilde{j}_{a}^{1} \end{pmatrix} = \begin{pmatrix} P_{\eta} & Q_{\eta} & R_{\eta} & S_{\eta} \\ P_{c} & Q_{c} & R_{c} & S_{c} \\ P_{q} & Q_{q} & R_{q} & S_{q} \\ P_{j} & Q_{j} & R_{j} & S_{j} \end{pmatrix} \begin{pmatrix} \tilde{\eta}_{b}^{1} \\ \tilde{c}_{b}^{1} \\ \tilde{N}_{b}^{1} \\ \tilde{j}_{b}^{1} \end{pmatrix}$$
[14]

or, since $a_n = b_{n+1}$ (Fig. 1), simply as

$$\mathbf{y}_{n+1} = \mathbf{M}_n \mathbf{y}_n \tag{15}$$

where y_n , y_{n+1} are the column vectors on the right and left sides of Eq. 14, respectively, and \mathbf{M}_n is the *n*th local matrix in Eq. 14 with the elements calculated in the middle of the interval $[a_n, b_n]$, i.e. at $\tilde{x} = (a_n + b_n)/2.$

From Eq. 15 it is evident that the recurrent solution process discussed in the previous section can be expressed in matrix notations as

$$\mathbf{y}_{N} = \mathbf{M}_{N}(\mathbf{M}_{N-1}...(\mathbf{M}_{2}(\mathbf{M}_{1}\mathbf{y}_{1}))...)$$
 [16]

Since the matrix multiplication is associative, Eq. 16 can be simplified to

$$\mathbf{y}_{N} = \mathbf{U}\mathbf{y}_{1},\tag{17}$$

where **U** is the product of N matrices

$$\mathbf{U} = \mathbf{M}_N \mathbf{M}_{N-1} ... \mathbf{M}_1. \tag{18}$$

and

$$\mathbf{y}_{1} \equiv (\tilde{\eta}_{1}^{1}, \, \tilde{c}_{1}^{1}, \, \tilde{N}_{1}^{1}, \, 0)^{T}$$
 [19]

is the column vector of unknowns at $\tilde{x} = 1$ (or, equivalently, for n=1). Note that the matrix **U** has to be calculated using Eq. 18 for each frequency ω .

The first two components $\tilde{\eta}_1^1$ and \tilde{c}_1^1 of the vector \mathbf{y}_1 are usually known (see next Section) and its fourth component is zero due to zero proton current through the CCL/GDL interface. The third component \tilde{N}_1^1 of \mathbf{y}_1 is unknown and it must provide zero oxygen flux at the membrane surface, leading to equation:

$$(\mathbf{U}\mathbf{y}_1)_3 = 0,$$
 [20]

i.e, the third component of vector Uy_1 must be zero. Writing Eq. 20 in components, we come to the linear algebraic equation

$$U_{31}\tilde{\eta}_1^1 + U_{32}\tilde{c}_1^1 + U_{33}\tilde{N}_1^1 = 0 ag{21}$$

with the solution

$$\tilde{N}_{1}^{1} = -\frac{1}{U_{33}} (U_{31} \tilde{\eta}_{1}^{1} + U_{32} \tilde{c}_{1}^{1}).$$
 [22]

where the double subscripts denote the row and column in U.

With U at hand, calculation of the CCL impedance for the frequency ω reduces to the following fast steps:

- Calculate \tilde{N}_1^1 using Eq. 22. Calculate the solution vector $\mathbf{y}_N = (\tilde{\eta}_N^1, \tilde{c}_N^1, \tilde{N}_N^1, \tilde{j}_N^1)^T$ at the membrane interface by multiplying 4×4 matrix **U** and vector \mathbf{y}_1 , Eq. 17. • Calculate the system impedance $\tilde{Z} = \tilde{\eta}_N^1/\tilde{j}_N^1$.

This sequence is repeated N_{ω} times, where N_{ω} is the number of frequency points in the spectrum. With the matrix U at hand, the first step gives \tilde{N}_1^1 directly. In terms of calculations speed, it provides a significant advantage over the recurrent method³⁴ employing iterative SciPy solver fsolve and Eq. 11. The pre-calculated U can also be reused in problems with different boundary conditions at $\tilde{x} = 1$.

Matrix U transforms the vector of boundary values \mathbf{y}_1 at $\tilde{x} = 1$ into the vector of solution \mathbf{y}_N at the single point $\tilde{x} = 0$, as required for impedance calculation. If the full solution shape along \tilde{x} is needed, the following algorithm does the job:

- Compute local matrices \mathbf{M}_n , n = 1, ..., N using the relations for matrix elements.34
- Calculate matrix U using Eq. 18.
- Calculate \tilde{N}_1^1 from Eq. 22.
- Use the recurrent formula, Eq. 15, to calculate the solution at all mesh points.

Incorporation of the gas diffusion layer impedance.—The oxygen concentration perturbation at the CCL/GDL interface, \tilde{c}_{i}^{1} in Eq. 21 allows us to incorporate GDL oxygen transport impedance into the model. With the dimensionless variables 5, equation for the oxygen concentration perturbation in the GDL $\tilde{c}_{\varrho}^{1}(\tilde{x}, \tilde{\omega})$ reads³³

$$\varepsilon^{2} \tilde{D}_{g} \frac{\partial^{2} \tilde{c}_{g}^{1}}{\partial \tilde{x}^{2}} = i \tilde{\omega} \mu^{2} \tilde{c}_{g}^{1}, \quad \tilde{D}_{g} \frac{\partial \tilde{c}_{g}^{1}}{\partial \tilde{x}} \bigg|_{\tilde{x}=1+} = \tilde{D}_{ox} \frac{\partial \tilde{c}^{1}}{\partial \tilde{x}} \bigg|_{\tilde{x}=1-},$$

$$\tilde{c}_{g}^{1} (1 + \tilde{l}_{g}) = \tilde{c}_{h}^{1} \tag{23}$$

where $\tilde{D_g}$ if the GDL oxygen diffusivity, \tilde{c}_g^1 , \tilde{c}_h^1 are the oxygen concentration perturbations in the GDL and channel, respectively, $\tilde{l}_g = l_g/l_t$ is the dimensionless GDL thickness. The left boundary condition for Eq. 23 means continuity of the oxygen flux at the CCL/GDL interface, and the right boundary condition expresses continuity of the oxygen concentration at the GDL/channel interface. Solution of Eq. 23 gives the oxygen concentration perturbation on the GDL side of the CCL/GDL interface:³³

$$\begin{split} \tilde{c}_g^1(1) &= -\frac{\tanh{(\tilde{l}_g q_*)}}{\tilde{D}_g q_*} \tilde{D}_{ox} \tilde{N}_1^1 + \frac{\tilde{c}_h^1}{\cosh{(\tilde{l}_g q_*)}}, \\ \text{where } q_* &\equiv \mu \sqrt{\mathrm{i}\tilde{\omega}/(\varepsilon^2 \tilde{D}_g)} \,. \end{split}$$
 [24]

Parameter \tilde{c}_h^1 in Eq. 24 provides the "interface" for incorporation of oxygen transport in the channel impedance. This option is not considered here; for the case of infinite (large) air flow stoichiometry, we set $\tilde{c}_h^1 = 0$.

Continuity of the oxygen concentration prescribes that $\tilde{c}_1^1 = \tilde{c}_g^1(1)$ and hence Eq. 24 with $\tilde{c}_h^1 = 0$ can be substituted for \tilde{c}_1^1 into Eq. 21. Solving Eq. 21, we get

$$\tilde{N}_{1}^{1} = \frac{U_{31}\eta_{1}^{1}}{U_{32}\alpha\tilde{D}_{ox} - U_{33}}, \quad \tilde{c}_{1}^{1} = -\alpha\tilde{D}_{ox}\tilde{N}_{1}^{1},$$
where $\alpha \equiv \tanh{(\tilde{l}_{g}q_{*})/(\tilde{D}_{g}q_{*})}$ [25]

With Eq. 25, vector \mathbf{y}_1 in Eq. 17 is fully determined.

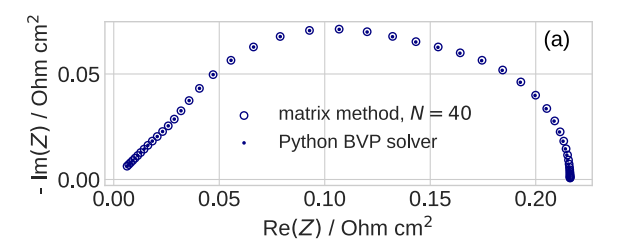
Numerical Results and Discussion

Figure 2 compares the impedance spectra obtained from the solution of Eqs. 3, 4 using the Python BVP solver solve_bvp and using Eq. 25 and the matrix equation 17 with N = 40 sub-layers. As can be seen, the matrix method quite accurately reproduces the exact numerical result. Parameters for the calculations are collected in Table I. Table II compares runtime of the three codes for impedance calculation with (i) the standard Python BVP solver, (ii) the recurrent solver, and (iii) the matrix solver. For this particular problem, at the cell current density of 1 A cm⁻², the recurrent solver is nearly three times faster than the standard Python BVP solver solve_bvp, while the matrix solver returns the spectrum 14.5 times faster than solve bvp. Fivefold acceleration of the matrix code as compared to the recurrent one is achieved thanks to direct calculation of parameter \tilde{N}_1^1 from Eq. 25. Note that in all the cases, nonlinear problem for the static shapes $\tilde{\eta}^0(\tilde{x})$ and $\tilde{c}^0(\tilde{x})$ was solved using *solve_bvp* and the respective computational time was excluded from the timing in Table II. At 0.1 A cm⁻², the advantage of matrix method over the BVP solver reaches nearly two orders of magnitude (Table II).

The accuracy of $\tilde{\eta}^0(\tilde{x})$ and $\tilde{c}^0(\tilde{x})$ stepwise approximation used in the recurrent and matrix methods depends on the cell current density. Due to the selected low CCL oxygen diffusivity (Table I) the oxygen concentration rapidly drops toward the membrane (Fig. 3). This dramatic decay together with the exponential variation of the parameter $e^{\tilde{\eta}^0}$ along \tilde{x} requires a large number N=40 of mesh points for the recurrent and matrix algorithms.

Figure 4 shows the residual error r of the matrix method

$$r = \|\tilde{Z}_{bvp} - \tilde{Z}_U\| \tag{26}$$



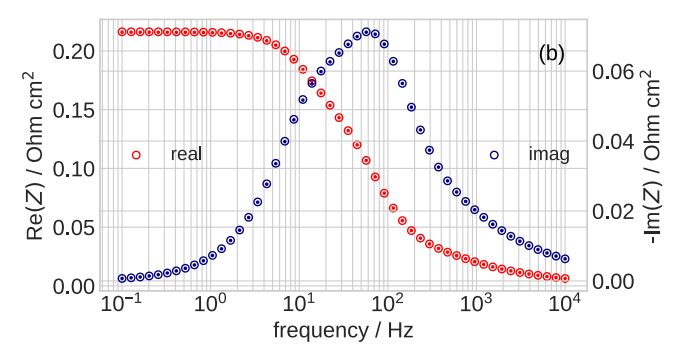


Figure 2. (a) Comparison of the Nyquist spectra obtained directly from Eqs. 3, 4 using Python BVP solver $solve_bvp$ (solid points) and the matrix method with N=40 mesh points (open circles). (b) Bode plots of the real and imaginary parts of the spectra in (a). The cell current density is 1 A cm⁻²; the other parameters are listed in Table I.

Table I. The cell parameters used in calculations.

CCL thickness l_t , cm	$10 \cdot 10^{-4}$
GDL thickness l_g , cm	$230 \cdot 10^{-4}$
CCL oxygen diffusivity D_{ox} , cm ² s ⁻¹	$1 \cdot 10^{-4}$
GDL oxygen diffusivity D_{GDL} , cm ² s ⁻¹	0.02
CCL proton conductivity σ_p S cm ⁻¹	0.01
ORR Tafel slope b_T , mV / exp	30
Double layer capacitance C_{dl} , F cm ⁻³	20
Cell current density j_0 , A cm ⁻²	1.0
Pressure	Standard
Cell temperature T, K	273 + 80

Table II. Comparison of the relative speed of impedance Z calculation for the cell current densities of 1 and 0.1 A cm⁻². In both the cases, unit is the speed of Z calculation from numerical solution of Eqs. 3, 4 using a standard Python BVP solver. The recurrent and matrix methods employed N=40 sub-intervals for $j_0=1$ A cm⁻² and N=10 for $j_0=0.1$ A cm⁻². The number of frequency points is 50 (10 points per decade).

Method	BVP solver Eqs. 3, 4	Recurrent method Eq. 11	Matrix solver Eq. 17
Relative speed of calculations			
at $j_0 = 1 \text{ A cm}^{-2}$	1	2.8	14.5
at $j_0 = 0.1 \text{ A cm}^{-2}$	1	7.5	53

where \tilde{Z}_{bvp} is the impedance obtained from the BVP solver, and \tilde{Z}_U is the impedance resulted from the matrix method. Doubling of the mesh points number reduces r by a factor of 4. In addition, r strongly depends on the cell current density j_0 : doubling of j_0 increases r by a factor of 5 to 7 (Fig. 4). Overall, doubling of the cell current requires

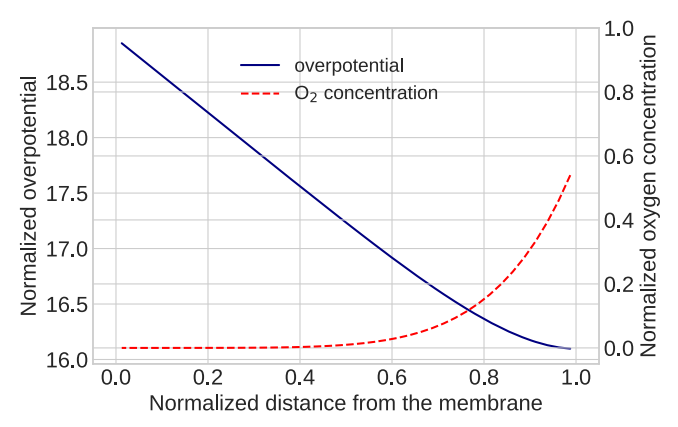


Figure 3. The static shapes of the dimensionless overpotential and oxygen concentration used in calculations of the spectra in Fig. 2.

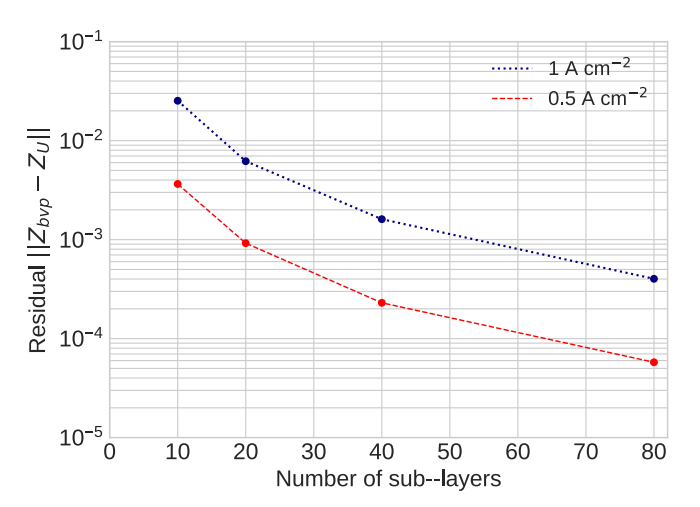
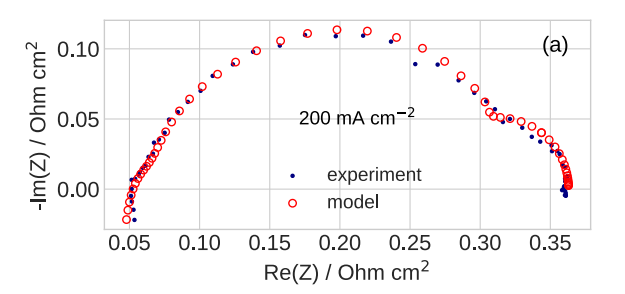


Figure 4. The residual error of the matrix method, Eq. 26, vs the number of sub-layers (numerical cells) for the cell current densities of 0.5 and 1 A cm^{-2} .

about twice more sub-layers to keep the same residual error. At lower currents, the gradients of \tilde{c}^0 and $\tilde{\eta}^0$ along \tilde{x} are small and N=20 or N=10 is quite sufficient for accurate spectra calculation (Fig. 4). In the latter case, the matrix method yields impedance up to two orders of magnitude faster than the standard BVP solver. For example, with the parameters in Table I, for the cell current density of $0.1~{\rm A~cm}^{-2}$ and N=10, the matrix solver returns quite accurate impedance spectrum 53 times faster than the BVP solver (Table II). It is worth noting that the matrix formulation can be easily extended for a nonuniform mesh, to resolve large local gradients of the static \tilde{c}^0 and $\tilde{\eta}^0$ shapes.

Figure 5 shows the experimental and fitted model spectra of a standard PEMFC with the cathode Pt loading of $0.4 \,\mathrm{mg}_{Pt} \,\mathrm{cm}^{-2}$. The main operating parameters are indicated in Fig. 5 caption; the other experimental details can be found in Ref. 35. The spectra have been fitted using the model, which takes into account the variation of oxygen concentration along the channel. The system of Eqs. solved includes Eqs. 3, 4, where \tilde{c}_1^1 is given by Eq. 24 with \tilde{c}_h^1 determined from equation for oxygen transport in the channel. The model was fitted to experiment using (i) the BVP solver and (ii) the matrix solver with N=20 mesh points. The fitted spectra from the two methods are visually indistinguishable. The fitting parameters from the two methods are compared in Table III. As can be seen, the parameters giving by the matrix solver are very close to those obtained with the BVP solver. However, the matrix solver returns the results 50 times faster than the Python BVP code solve_bvp.



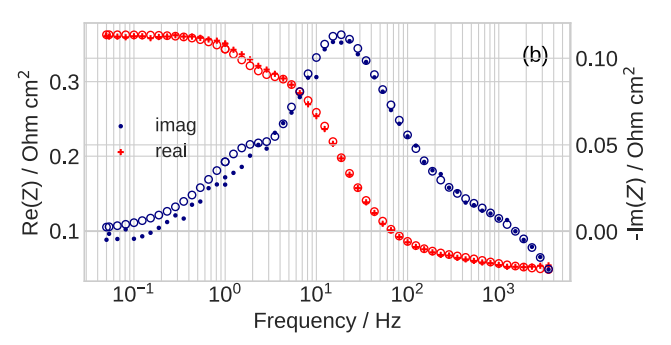


Figure 5. (a) Experimental (points) and fitted model (open circles) Nyquist spectra of a standard PEM fuel cell at the cell current density of 200 mA cm⁻², cell temperature 80 °C, cathode absolute pressure 1.5 bar, cathode RH 50%. The anode/cathode feed gases are hydrogen/air at 2/4 stoichiometry. The other experimental details can be found in Ref. 35. (b) The frequency dependence of imaginary and real parts of the spectra in (a).

Table III. Comparison of the fitting parameters for the model spectrum in Fig. 5 resulted from the BVP and matrix solvers in the least-squares fitting procedure. With the matrix solver, the results are obtained 50 times faster, than with the standard Python BVP-solver.

	BVP solver	Matrix solver
ORR Tafel slope b_T , mV	32.9	33.3
CCL proton conductivity σ_p , mS cm ⁻¹	11.9	13.4
DL capacitance C_{dl} , F cm ⁻³	21.7	21.6
CCL oxygen diffusivity D_{ox} , cm ² s ⁻¹	0.729×10^{-4}	0.750×10^{-4}

Generally, the matrix solver can be developed for any linear BVP with variable coefficients, provided that the reasonably simple analytical solution of this BVP with constant coefficients can be derived. This implies some preliminary analytical work to obtain solution of the respective Cauchy problem analogous to (9), (10), resulting in explicit expressions for the matrix elements in Eqs. 11. As soon as the coefficients in Eq. 11 are known, the matrix U for the given problem can be calculated. Due to BVP linearity, missing elements of vector \mathbf{y}_1 can be directly expressed though the elements of matrix U and available \mathbf{y}_1 components using the boundary conditions at $\tilde{x}=1$. With \mathbf{y}_1 and local matrices \mathbf{M}_n , fast calculation of the solution at all mesh points is described in the last paragraph of Matrix formulation Section.

Conclusions

A fast matrix solver of a boundary–value problem for a system of two linear complex–valued ODEs with variable coefficients is developed. To this end, solution of the respective Cauchy problem on a small interval $\tilde{x} \in [a_n, b_n]$ is derived, assuming that the ODE coefficients on this interval are constant. Analytical solution of the Cauchy problem gives a system of four linear algebraic equations relating the unknown functions and their derivatives on either side of the interval. By writing the algebraic system in matrix form, in

becomes evident that solution of the underlying BVP reduces to the product of local 4×4 matrices, which is computationally fast procedure not requiring iterations.

The method is applied to solve the core physics—based model for PEM fuel cell impedance, which includes proton transport in the cathode catalyst layer and oxygen transport in the CCL and GDL. Numerical test shows that for the cell current density of 1 A cm⁻² and low CCL oxygen diffusivity, the matrix method with 40 mesh points returns the PEMFC impedance 14.5 times faster than the standard Python boundary—value problem solver *solve_bvp*. For lower cell currents, the gain in the computation speed reaches nearly two orders of magnitude. Least—squares fitting of the experimental impedance spectrum measured at the cell current density of 200 mA cm⁻² shows that the code with the matrix method returns results 50 times faster than the code based on a standard BVP solver. This makes the core physics—based impedance model with the matrix solver a fast and robust alternative to the widely used equivalent circuit modeling.

Acknowledgments

The author is grateful to Dr. Tatyana Reshetenko (University of Hawaii) for the experimental data in Fig. 5 and many useful discussions.

ORCID

Andrei Kulikovsky https://orcid.org/0000-0003-1319-576X

References

- A. Lasia, Electrochemical Impedance Spectroscopy and its Applications (Springer, New York) (2014).
- Z. Tang, Q.-A. Huang, Y.-J. Wang, F. Zhang, W. Li, A. Li, L. Zhang, and J. J. Zhang, "Recent progress in the use of electrochemical impedance spectroscopy for the measurement, monitoring, diagnosis and optimization of proton exchange membrane fuel cell performance." *J. Power Sources*, 468, 228361 (2020).
- D. Macdonald, "Reflections on the history of electrochemical impedance spectroscopy," *Electrochim. Acta.* 51, 1376 (2006).
- R. M. Fuoss and J. G. Kirkwood, "Electrical properties of solids. viii. Dipole moments in polyvinyl chloride-diphenyl systems." J. Am. Chem. Soc., 63, 385 (1941).
- H. Schichlein, A. C. Müller, M. Voigts, A. Krügel, and E. Ivers-Tiffée, "Deconvolution of electrochemical impedance spectra for the identification of electrode reaction mechanisms in solid oxide fuel cells." *J. Appl. Electrochem.*, 32, 875 (2002).
- M. Saccoccio, T. H. Wan, C. Chen, and F. Ciucci, "Optimal regularization in distribution of relaxation times applied to electrochemical impedance spectroscopy: Ridge and lasso regression methods - a theoretical and experimental study." *Electrochim. Acta*, 147, 470 (2014).
- E. Ivers-Tiffée and A. Weber, "Evaluation of electrochemical impedance spectra by the distribution of relaxation times." J. Ceramic Soc. Japan, 125, 193 (2017).
- B. A. Boukamp, "Distribution (function) of relaxation times, successor to complex nonlinear least squares analysis of electrochemical impedance spectroscopy?" *J. Phys. Energy*, 2, 042001 (2020).
- J. Song and M. Z. Bazant, "Electrochemical impedance imaging via the distribution of diffusion times." *Phys. Rev. Lett.*, 120, 116001 (2018).
- A. Kulikovsky, "A model-based analysis of PEM fuel cell distribution of relaxation times." *Electrochim. Acta*, 429, 141046 (2022).
- 11. A. Lasia, "Impedance of porous electrodes." J. Electroanal. Chem., 397, 27 (1995).
- T. E. Springer, T. A. Zawodzinski, M. S. Wilson, and S. Gottesfeld, "Characterization of polymer electrolyte fuel cells using AC impedance spectroscopy." J. Electrochem. Soc., 143, 587 (1996).

- M. Eikerling and A. A. Kornyshev, "Electrochemical impedance of the cathode catalyst layer in polymer electrolyte fuel cells." *J. Electroanal. Chem.*, 475, 107 (1999).
- Y. Bultel, L. Genies, O. Antoine, P. Ozil, and R. Durand, "Modeling impedance diagrams of active layers in gas diffusion electrodes: Diffusion, ohmic drop effects and multistep reactions." J. Electroanal. Chem., 527, 143 (2002).
- F. Jaouen and G. Lindbergh, "Transient techniques for investigating mass-transport limitations in gas diffusion electrode." *J. Electrochem. Soc.*, 150, A1699 (2003).
- Q. Guo and R. E. White, "A steady-state impedance model for a PEMFC cahode." J. Electrochem. Soc., 151, E133 (2004).
- S. Devan, V. R. Subramanian, and R. E. White, "Analytical solution for the impedance of a porous electrode." *J. Electrochem. Soc.*, 151, A905 (2004).
- S. K. Roy, M. E. Orazem, and B. Tribollet, "Interpretation of low-frequency inductive loops in PEM fuel cells." J. Electrochem. Soc., 154, B1378 (2007).
- D. Gerteisen, A. Hakenjos, and J. O. Schumacher, "AC impedance modelling study on porous electrodes of proton exchange membrane fuel cells using an agglomerate model." *J. Power Sources*, 173, 346 (2007).
- M. Mathias, D. Baker, J. Zhang, Y. Liu, and W. Gu, "Frontiers in application of impedance diagnostics to H₂-fed polymer electrolyte fuel cells." *ECS Trans.*, 13, 129 (2008).
- I. A. Schneider, M. H. Bayer, and S. von Dahlen, "Locally resolved electrochemical impedance spectroscopy in channel and land areas of a differential polymer electrolyte fuel cell." *J. Electrochem. Soc.*, 158, B343 (2011).
- 22. G. Maranzana, J. Mainka, O. Lottin, J. Dillet, A. Lamibrac, A. Thomas, and S. Didierjean, "A proton exchange membrane fuel cell impedance model taking into account convection along the air channel: on the bias between the low frequency limit of the impedance and the slope of the polarization curve." *Electrochim. Acta*, 83 13 (2012)
- S. Tant, S. Rosini, P.-X. Thivel, F. Druart, A. Rakotondrainibe, T. Geneston, and Y. Bultel, "An algorithm for diagnosis of proton exchange membrane fuel cells by electrochemical impedance spectroscopy." *Electrochim. Acta*, 135, 368 (2014).
- B. P. Setzler and T. Fuller, "A physics-based impedance model of proton exchange membrane fuel cells exhibiting low-frequency inductive loops." *J. Electrochem.* Soc., 162, F519 (2015).
- A. Baricci and A. Casalegno, "A simple analytical approach to simulate the electrochemical impedance response of flooded agglomerates in polymer fuel cells." *Electrochim. Acta*, 157, 324 (2015).
- C. Bao and W. G. Bessler, "Two-dimensional modeling of a polymer electrolyte membrane fuel cell with long flow channel. Part II. physics-based electrochemical impedance analysis." J. Power Sources, 278, 675 (2015).
- D. Gerteisen, "Impact of inhomogeneous catalyst layer properties on impedance spectra of polymer electrolyte membrane fuel cells." *J. Electrochem. Soc.*, 162, F1431 (2015).
- T. Reshetenko and A. Kulikovsky, "Comparison of two physical models for fitting PEM fuel cell impedance spectra measured at a low air flow stoichiometry." J. Electrochem. Soc., 163, F238 (2016).
- S. Chevalier, C. Josset, and B. Auvity, "Analytical solution for the low frequency polymer electrolyte membrane fuel cell impedance." *J. Power Sources*, 407, 123 (2018).
- A. Kosakian and M. Secanell, "Estimating charge-transport properties of fuel-cell and electrolyzer catalyst layers via electrochemical impedance spectroscopy." *Electrochim. Acta*, 367, 137521 (2021).
- J. Huang, Y. Gao, J. Luo, S. Wang, C. Li, S. Chen, and J. Zhang, "Editors' choice-review-impedance response of porous electrodes: theoretical framework, physical models and applications." J. Flortzechem. Soc. 167, 166503 (2020).
- physical models and applications." *J. Electrochem. Soc.*, 167, 166503 (2020).
 T. Reshetenko and A. Kulikovsky, "Impedance spectroscopy characterization of oxygen transport in low- and high-pt loaded PEM fuel cells." *J. Electrochem. Soc.*, 164, F1633 (2017).
- A. Kulikovsky, "Analytical impedance of PEM fuel cell cathode including oxygen transport in the channel, gas diffusion and catalyst layers." J. Electrochem. Soc., 169, 034527 (2022).
- A. Kulikovsky, "A fast recurrent model for high-current PEM fuel cell impedance." J. Electrochem. Soc., 170, 044506 (2023).
- T. Reshetenko and A. Kulikovsky, "Variation of PEM fuel cell physical parameters with current: Impedance spectroscopy study." J. Electrochem. Soc., 163, F1100 (2016).
- T. Reshetenko and A. Kulikovsky, "A model for extraction of spatially resolved data from impedance spectrum of a PEM fuel cell." J. Electrochem. Soc., 165, F291 (2018).